J Mater Sci (2007) 42:3789–3799
DOI 10.1007/s10853-006-0413-0

Candidate mechanisms controlling the electrical characteristics of silica/XLPE nanodielectrics

Mihir Roy · J. Keith Nelson · R. K. MacCrone · L. S. Schadler

Received: 3 February 2006 / Accepted: 5 May 2006 / Published online: 11 February 2007

Abstract The incorporation of silica nanoparticles into polyethylene has been shown to increase the breakdown strength significantly compared to composites with micron scale fillers. Additionally, the voltage endurance of the nanocomposites is two orders of magnitude higher than that of the base polymer. The most significant difference between micron-scale and nano-scale fillers is the large interfacial area in nanocomposites. Because the interfacial region (interaction zone) is likely to be pivotal in controlling properties, this paper compares the behavior of nanoscale silica/cross-linked low density polyethylene nanocomposites with several silica surface treatments. In addition to breakdown strength and voltage endurance, dielectric spectroscopy, absorption current measurements, and thermally stimulated current determinations (TSC) were performed to elucidate the role of the interface. It was found that a reduction in the mobility in nanocomposites as well as a change in the defect size may be key to explaining the improvement in the properties.

M. Roy · R. K. MacCrone · L. S. Schadler (✉)
Materials Science and Engineering Department,
Rensselaer Polytechnic Institute,
Troy, NY 12180, USA
e-mail: schadl@rpi.edu

J. K. Nelson
Electrical, Computer, and Systems Engineering
Department, Rensselaer Polytechnic Institute,
Troy, NY 12180, USA

Introduction

Nanocomposite-dielectrics, or nanodielectrics, can exhibit dielectric properties that are better than the base polymer and significantly better than conventional composites with micron scale filler. For example, an increase in dielectric strength and an accompanying reduction in space charge has been documented for the case of nano-TiO_2 filled epoxy resin compared to micron scale TiO_2 filled epoxy composites [1] and titania filled low density polyethylene (LDPE) composites compared to micron scale TiO_2 filled LDPE composites [2]. In the nano-TiO_2 filled epoxy composites, the electrical voltage endurance was three orders of magnitude higher than that of the base resin [3]. The improvements in nanocomposite electrical behavior have been attributed to (i) changes in the space charge distribution [4, 5], (ii) a reduction in the internal field caused by the decrease in particle size, and (iii) changes in the polymer morphology [2].

The particle–polymer interface is critical in determining the properties of nano-filled materials because at the same particle loading, nanocomposites have a much greater interfacial area than microcomposites. Since a significant percentage of polymer will be in these interfacial areas (zones), the properties of the overall composite will be dominated by the interfacial properties [6] even at low volume fractions of filler [7, 8]. Some authors have emphasized that the interaction zone around the particles is a ''quasi-conductive'' region that partially overlaps in the nanocomposites [9]. These overlapped interface regions may allow charge dissipation, which, in turn, could be expected to improve the dielectric breakdown strength and voltage endurance characteristics by improving the internal

electric field distribution. It has been shown that when the size of the filler approaches the chain conformation length, they act 'cooperatively' with the host structure either eliminating or suppressing Maxwell–Wagner polarization, which is well known in the case of conventionally filled materials [1]. Introduction of a second phase can also influence the breakdown strength of the dielectrics via a scattering mechanism [10] (i.e., a decrease in path length of the carriers responsible for the breakdown processes), or by changing the space charge distribution [11].

Although the importance of the size of the filler in determining the global properties (electrical, mechanical and thermal) is undeniable [12], the chemistry of the particle surface is also critical. The addition of molecules that are more or less compatible with the matrix and with a polar or non-polar nature will impact the breakdown strength. In addition, the changes in morphology due to incorporating nanoparticles, particularly for semicrystalline polymers are of enormous importance [13, 14]. The breakdown strength of the intraspherulitic regions is higher than that of the interspherulitic regions and a change in the disorder within the spherulites or of the interspherulitic region can affect the breakdown strength.

The promise of unique electrical properties due to the mechanisms just described provides an incentive for investigating the dielectric properties of nano-filled materials. This study of a silica/cross-linked polyethylene (XLPE) system [15] has found a significant increase in breakdown strength in the nanoscale composites as well as a two orders of magnitude increase in the voltage endurance compared to the unfilled XLPE. Using XPS (X-ray photoemission spectroscopy) and EPR (electron paramagnetic resonance) to characterize the interface, as well as dielectric spectroscopy and space charge measurements to understand the internal electrical response, two main differences between the nanofilled and micron filled materials that were relevant have been hypothesized. First, in the case of untreated fillers, it appears that there may be a quasi-conductive region surrounding the nanoparticles that provided an opportunity for charge dissipation. This is supported by the dielectric spectroscopy data. Second, the covalent bonding between functionalized nanoparticles and the XLPE was one of the keys to the improved voltage endurance. It has been concluded that any changes in crystallinity were not the primary mechanism controlling dielectric breakdown.

In this paper, some of the earlier results are reviewed to provide an opportunity to compare the behavior for several different interface conditions. Additionally, new results on the absorption current and thermally stimulated depolarization provide some understanding of the silica/XLPE system. A statistical analysis of the data using defect size distribution provides further insight into the electrical failure behavior. Finally, by drawing on the full set of data, some conclusions are advanced about the dominant mechanisms controlling dielectric breakdown and voltage endurance of nanofilled polymers.

Systems investigated

Polyethylene–SiO_2 composites were formulated using micron and nanoscale particulates. The base polyethylene used for the matrix is a commercially available material used in the manufacturing of high-voltage (HV) extruded cross-linked underground cables. It contains antioxidants (non-ionic and hence, do not contribute to the base polymer conductivity) and a cross-linking agent, dicumyl peroxide (DCP), which reacts at temperatures above the compounding temperature creating a cross-linked matrix.

The nanosilica was either used untreated or was commercially surface-modified with triethoxyvinylsilane (TES), *n*-(2-aminoethyl) 3-aminopropyltrimethoxysilane (AEAPS), or hexamethyldisilazane (HMDS). The structures of these compounds are depicted in Fig. 1. AEAPS and HMDS are both polar molecules creating an incompatible interface with the XLPE and possibly causing scattering or charge trapping. TES is non-polar and provides an opportunity for covalent bonding (and thus a strong interface) with the matrix. Prior work [15] showed that the vinylsilane treatment indeed resulted in covalent bonding between the particles and the polymer.

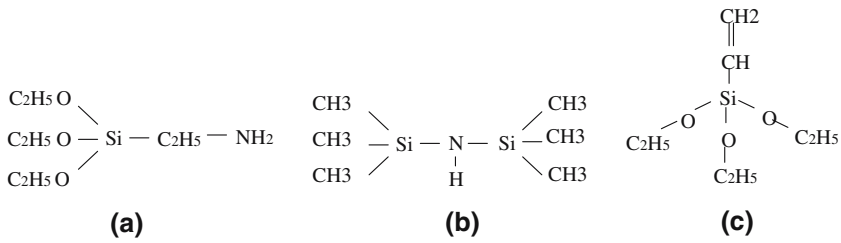

Fig. 1 Schematic depicting atomic arrangements in the three surface modifiers; (**a**) aminopropyltrimethoxysilane (AEAPS), (**b**) hexamethyldisilazane (HMDS) and (**c**) vinylsilane (TES)

The particles and polyethylene were melt mixed until the aggregate size was less than 100 nm as measured using scanning electron microscopy. All the composites were loaded with 5 wt% of nanoparticles. The details of sample formulations are discussed in [15]. In brief, the particles were vacuum dried for 24 h immediately prior to compounding. All samples were created by hot pressing, and then allowed to cool slowly to room temperature, keeping the pressure constant. The samples were post-cured under vacuum which is important since cross-linking byproducts may otherwise affect the electrical properties. The samples meant for electrical testing were metallized with ~150 Å of sputtered gold. Melt processing and post-cure annealing are likely to mitigate the presence of pre-existing electric charge.

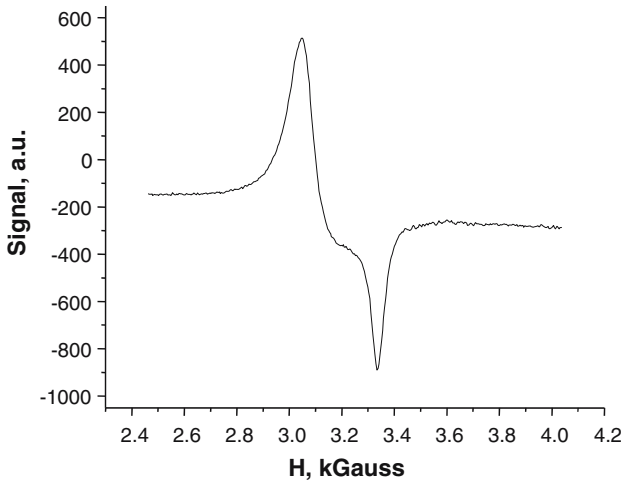

Fig. 2 EPR derivative spectra of the untreated nanosilica particles

Characterization of particles

Electron Paramagnetic Resonance (EPR) spectra were used to detect differences in the particle defect density as a function of surface treatment and composite compounding. All the powdered silica samples and composites (cryo-crushed) were measured using a Bruker ER 042 EPR spectrometer. In the simplest case, the resonance condition is given by:

$$Hv = gbH, \tag{1}$$

where H is the magnetic field, b is the Bohr magneton, and v is the frequency of the microwave radiation, and g is the Lande factor. For a spin only electron, $g = 2.0023$. The magnetic field was measured using a Walker Hall probe Tesla meter, the instrument being set at one value using the resonance of diphenyl picryl hydrazyl (dpph), which has a g value of 2.0034, as a standard. The magnetic field values are accurate to within 0.01%. The spectrometer measures the derivative of the absorption at X-band, the frequency, being in the range 9.77 GHz.

We show the derivative spectrum of untreated silica nanoparticles (Fig. 2). This spectrum is typical of all spectra obtained from our different samples. The overall magnitude in the spectra obtained varies between differently treated specimens. Subtle differences in spectral shape are also exhibited. Considering the composition of the particles, the paramagnetic species responsible here are most likely oxygen radical species. Oxygen radicals in dilute systems, where complicating magnetic interactions are not present, are well known. All oxygen radical spectra are each characterized by three tensorial g-values ranging between 2.0 and 2.4. These values can be determined from the resulting complex spectra, with several well-defined maxima and minima. In our case, these complexities averaged out and are not observed. This may come about for several reasons. First, in our case the number of oxygen radicals is large, implying strong dipole–dipole and exchange interactions. Some radicals may be especially close together due to structural considerations. In view of the glass-forming ability of silica, there are also likely to be wide structural variation between the sites of the several different radical species in question, such as {O–, O_2–, (O–)2, (OO)–} [16]. In addition considerable molecular motion may be taking place, so that structural reorientation on the microwave period time scale also contributes to broadening.

A detailed analysis of the spectra is presently in progress, and will be presented elsewhere. For present purposes, we have used the normalized spectra to monitor the oxygen radical content present in arbitrary units (a.u.) in Table 1. Power saturation and over modulation were determined to be absent. These radicals are presumed to be associated mostly with the particle surface. Significantly, we did not observe any E' centers associated with the silica particles. The EPR spectrum of this oxygen vacancy defect is very narrow, implying better detectability at very low content compared to oxygen radicals. The untreated silica nanoparticles have a much higher signal than the micron scale particles indicating much higher diatomic oxygen content. The surface-treated nanoparticles have an EPR signature similar to the micron scale particles, suggesting that the oxygen radicals were partly eliminated during the surface treatments. The

Table 1 Peak EPR signal for particulates and 5 wt% composites

Material	Signal (a.u.)	
	SiO_2	Composite
Micron Scale silica	550	1,600
Nanoscale silica	6,000	6,600
AEAPS treated nanosilica	250	1,600
HMDS treated nanosilica	550	600
TES treated nanosilica	550	1,300

number of radicals increases when the particles are incorporated into the polymer. This is true for all types of particles. Although the resurgence of oxygen radicals is lower for the surface-treated nanosilica fillers compared to the untreated nanosilica fillers, the trend of increasing oxygen radicals in the composites is evident.

X-ray Photoelectron Spectroscopy (XPS) was utilized to investigate the surface chemistry characteristics for all the nanoparticles and microparticles. XPS analysis was done on a Perkin Elmer (Model # 5500) using MgK_α monochromatic radiation. Data were gathered before argon cleaning and after 3 min, 6 min and 9 min of argon cleaning; it was found that the data were similar in peak position and intensity. Data gathered were analyzed using Auger Scan-2 software, which employs a linear least squares optimization with a simplex peak-fitting algorithm. XPS analysis indicated that the surface of the particle contains mainly oxygen and silicon for the untreated particles and traces of nitrogen, in addition, for the surface treated particles. The four possible chemical structures of silicon in its four oxidation states (Si^{+}, Si^{2+}, Si^{3+} and Si^{4+}) were considered for analyzing the XPS data. The corresponding Si 2p binding energies were taken from the literature [17] and are given in Table 2. The Si-2p peak is fitted with a symmetrical Gaussian fit and in each fit the alternative peak positions were kept at the same width while the intensity was adjusted. From the intensity of the peaks the stoichiometric formula SiO_x was calculated using the formula:

$$x = \frac{\sum_{i=1}^{4} n_i H_i}{\sum_{i=1}^{4} H_i}, \tag{2}$$

where n is the oxidation state of silicon and H is the peak intensity. It was found that the oxygen content in all the surface treated nanosilica is of similar level (~1:1 ratio with silicon) and lower than that of the untreated nano- and micron-scale silica (~1.3:1 ratio with silicon).

Table 2 Silicon chemical environments and corresponding binding energies [15]

Structure	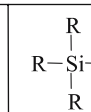	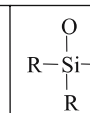	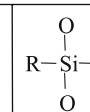	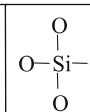
Abbreviation	$Si(-O)_1$	$Si(-O)_2$	$Si(-O)_3$	$Si(-O)_4$
Binding Energy (eV)	101.8	102.1	102.8	103.4

Electrical characterization

The DC breakdown strength was measured using recessed specimens with gold electrodes. A conventional 2-parameter Weibull distribution was used to analyze the breakdown data for samples ranging in thickness from 0.15 mm to 0.015 mm [18]. The recessed samples were created using a mold that allowed 25 samples to be prepared on a single wafer thereby allowing multiple specimens to be created simultaneously to permit the large number of breakdown measurements needed to obtain reliable estimates of stochastic parameters. The withstand strength was determined using a high-voltage source with a ramp rate of 500 V s^{-1} applied to the metallized electrodes in a thermostatically controlled enclosure. The cumulative probability P of the electrical failure takes the form of:

$$P = 1 - \exp\left[-\left(\frac{E}{E_0}\right)\right]^{\beta}, \tag{3}$$

where β is a shape parameter and E_0 is a scale parameter that represents the breakdown strength at the cumulative failure probability of 63.2%. Breakdown tests were conducted at four different temperatures (25 °C, 60 °C, 70 °C, and 80 °C).

Long-term voltage endurance tests were carried out using cylindrical blocks of polymer or polymer nanocomposites, embedded with a tungsten electrode of tip radius, r, of approximately 4 μm (for a highly divergent field) and 12 μm (for a less divergent field), with an inter-electrode distance, d, of ~2 mm. The samples were stressed with a 60 Hz alternating voltage, and the tip stress, E, was calculated from the applied voltage using the relationship [1]:

$$E = \frac{2V}{r\ln(4d/r)}. \quad (4)$$

The microcomposite voltage endurance was not tested because of its known poor breakdown performance.

Dielectric spectroscopic measurements of the samples were completed at 25 °C, 60 °C, 70 °C, and 80 °C using a Novocontrol Alpha Analyzer (type K) in combination with a Novocontrol active BDS-1200 sample cell. The laminar samples were approximately 0.5 mm thick with a gold electrode sputtered onto a circular area of 2.2 cm in diameter.

Thermally stimulated current (TSC) measurements were used to investigate the nature and the origin of charge carrier traps. The base polymer (XLPE) is well characterized using TSC [19]. TSC measurements were performed using laminar samples of thickness ~100 μm with sputtered deposited platinum electrodes on both sides. The poling temperature used for all samples was 60 °C and the temperature ramp rate for the TSC measurements was 2 °C/min from 40 °C to 100 °C. From the two sets of samples tested for each type of material, the peak position was found to be reproducible within ±1 °C.

When a DC field is applied to a finite thickness of non-ideal dielectric sandwiched between two plane parallel electrodes, the current decays slowly over time. This slowly decreasing current is referred to as the 'absorption current' or 'anomalous current'. Absorption current measurements were performed utilizing a Keithley 8009 Resistivity Test Fixture on laminar samples of thickness from 50 μm to 500 μm over a range of electric fields from 10^5 V/m to 3×10^7 V/m, and all measurements were performed at room temperature (298 ± 3 °K).

Results

One of the key factors controlling the electrical behavior in filled polymers is the particle dispersion. An extensive study of dispersion is not reported here, but the dispersion for all the samples was similar as observed using scanning electron microscopy. Small clusters of particles were observed (5–10 particles) but many of the particles were isolated. As mentioned, crystallinity can also affect the breakdown strength. Prior differential scanning calorimetry [15] data showed that the percent crystallinity is about 40% for the unfilled, micron scale composites, untreated nanoscale silica, AEAPS, and HMDS treated silica nanocomposites. The crystallinity for the vinylsilane-treated (TES) silica nanocomposites was about 60%. Previous reports [15] have shown that percent crystallinity is not a primary parameter in the behavior of these materials.

The characteristic breakdown strength for XLPE at room temperature is found to be about 270 kV/mm, which is comparable to published values [20]. There is a dramatic increase in breakdown strength for the untreated nanofilled composites over the micron-filled counterparts shown in Fig. 3. There is an incremental improvement in breakdown strength for the AEAPS and HMDS nanosilica composites. The TES nanosilica filled composites exhibit a still higher breakdown strength. In addition, the TES nanocomposite retained 50% of its breakdown strength at 80 °C, while the other composites saw a 70% decrease (Table 3).

The superior performance of the nanofilled material over the base resin is best demonstrated by a voltage endurance test. Figure 4 shows the relationship between electrode tip-stress versus lifetime. For tip stresses above 500 kV/mm, the XLPE breaks down almost immediately (within a matter of two hours,

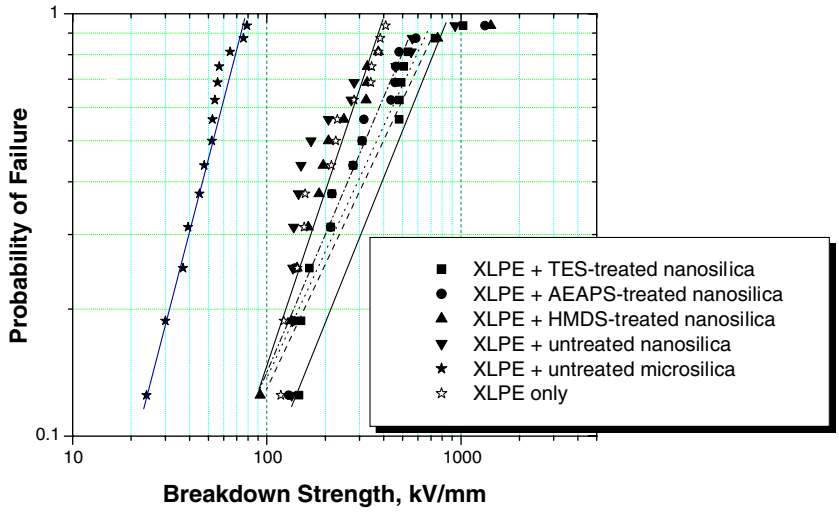

Fig. 3 Weibull plots of the breakdown probability of XLPE together with a variety of composites—Something wrong on the color of this plot… should be black and white

Table 3 Characteristic breakdown voltage (kV/mm) of XLPE and several nanocomposites at a range of temperatures (Weibull shape parameter in parenthesis)

Materials	Temperature			
	25 °C	60 °C	70 °C	80 °C
XLPE	269 (2.49)	183 (2.65)	129 (3.66)	79 (3.84)
XLPE + untreated nanosilica	314 (2.07)	260 (2.27)	213 (2.49)	83 (3.09)
XLPE + AEAPS treated nanosilica	400 (1.69)	266 (2.20)	263 (1.79)	134 (2.11)
XLPE + HMDS treated nanosilica	336 (1.69)	225 (1.97)	208 (2.14)	128 (2.09)
XLPE + TES treated nanosilica	446 (1.73)	422 (2.22)	344 (2.17)	220 (2.87)

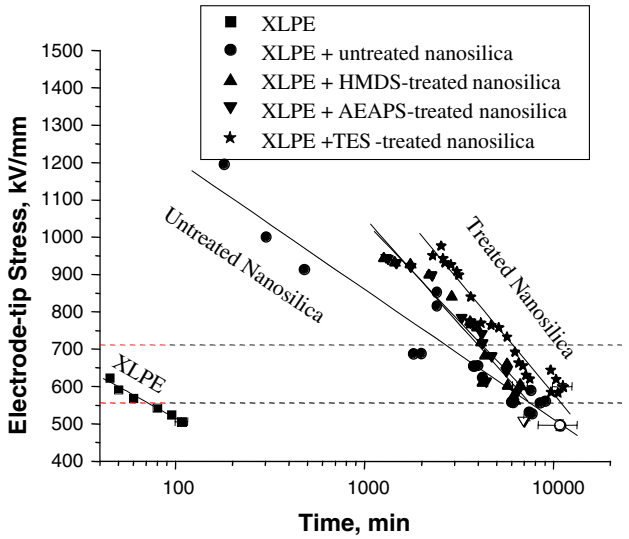

Fig. 4 Voltage endurance of XLPE and the untreated and functionalized nanocomposites

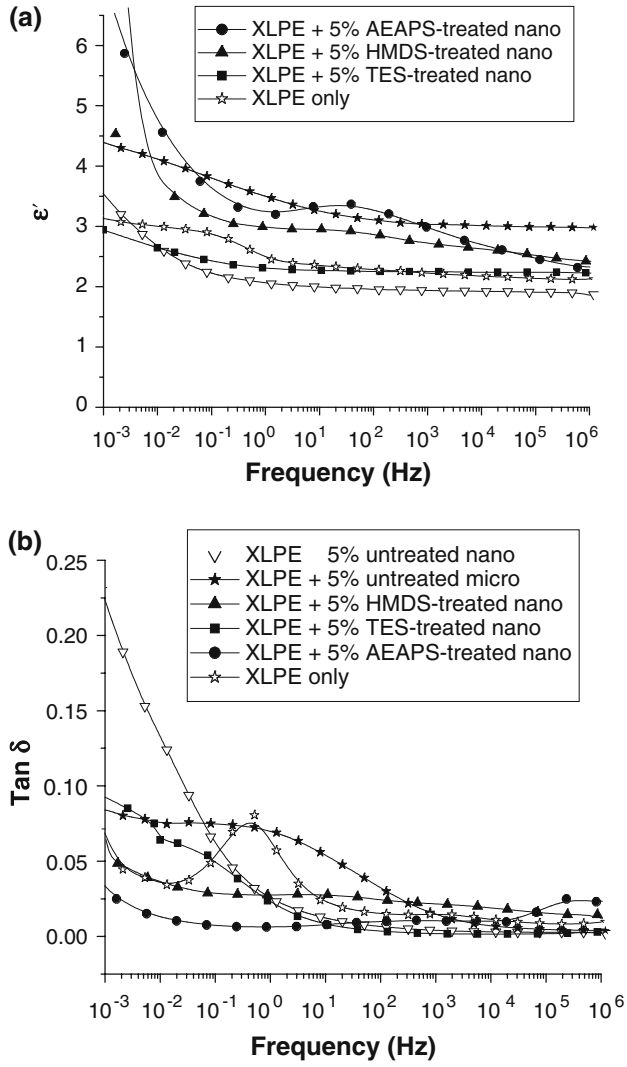

Fig. 5 (**a**) Dielectric permittivity and (**b**) loss tangent of XLPE and all the composites at room temperature

which is reduced to less than an hour at 600 kV/mm). In contrast, the filled materials exhibit a time to failure which is two orders of magnitude higher than the base resin. It is clear that the less divergent (more uniform) field specimens (represented as open symbols in Fig. 4) and the more divergent field specimens lead to similar endurance times at lower tip stress. Again, there was an incremental improvement in endurance time exhibited by the surface treated silica nanocomposites.

Figure 5 (a) and (b) show the change in permittivity and tan δ as a function of frequency at 25 °C for the base resin as well as the micron filled and nanofilled XLPE. The predicted permittivity of composites with 5 wt% of filler calculated using the Lichtenecker–Rother logarithmic formula [21], Maxwell–Garnet random mixing formula [22], and Landau–Lifshitz power law formula [23], with a power factor (exponential term in power law equation) of 1/3, yields approximately 2.23 (at 60 Hz). This is a little higher than the unfilled material. The microcomposites exhibited a much higher value of 3.14 suggesting that some interfacial polarization is present. The nanocomposites, however, showed values lower than that of the base resin (2.2). This is true at all temperatures (not shown in the figure). Figure 5(b) compares the loss tangent of the micron scale composites and nanocomposites. The

broad loss peak, which appears in the micron scale composites, is completely eliminated for all the nanocomposites. The nanoparticles appear to reduce the chain movement of the polymer through physical bonding or through confinement. In the case of untreated nanocomposites, the permittivity is unchanged for a given temperature for a wide range of frequency (0.1 Hz–1 MHz), but starts to increase due to 'quasi-DC' conduction [24] at lower frequencies. This 'quasi-DC' conduction at low frequency has been explained by Lewis [9] utilizing O'Konski's model [25] and a double layer approach. By this model, charge carriers are efficiently transferred around the interface by the field leading to an induced polarization at the polar ends of the particle which becomes a large dipole. This will lead to a dielectric constant higher than the particle itself. Since these double layer effects are likely to be pronounced in nanocomposites, the slope of the permittivity is steeper than for the microcomposite (which also has untreated fillers) in the low frequency region.

The real part of the permittivity (Fig. 5(a)) of the AEAPS and HMDS surface-treated nanosilica composites contains a peak above 1 Hz not present in the other materials. These peaks are not characteristics of adsorbed water, which shows a peak around 1 Hz, implying that they originate due to the surface modifiers. On the other hand, the tan δ behavior of the surface-treated nanocomposites is very different from the untreated nanocomposite (Fig. 5(b)) in the low frequency region. The slope of the 'quasi-DC' part demonstrated in the untreated nanofilled composite is completely absent in the surface-treated nanocomposites, suggesting that the conducting sheath present in the case of untreated nanofilled material is substantially affected by the coupling. The activation energy for the low frequency dispersion was calculated by the normalization method [24] by shifting the imaginary part of the frequency spectra laterally and then determining the frequency shift required to bring the curves into coincidence. The activation energy for each composite in Table 4 shows that the two polar surface-modified nanocomposites have a higher activation energy than the untreated and TES treated nanocomposites and marginally higher than microcomposite.

Table 4 Activation energies for all composites derived from dielectric spectroscopy

Sample name	Activation energy (eV)
XLPE + 5% untreated nanosilica	0.18 ± 0.05
XLPE + 5% AEAPS treated nanosilica	0.34 ± 0.07
XLPE + 5% HMDS-treated nanosilica	0.31 ± 0.04
XLPE + 5% TES treated nanosilica	0.18 ± 0.09
XLPE + 5% microsilica	0.28 ± 0.06

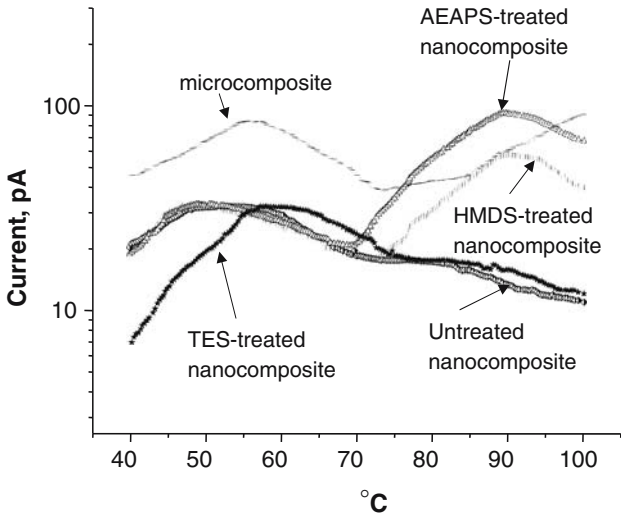

Fig. 6 Thermally stimulated Current spectra for silica-filled composites

Figure 6 shows TSC spectra for all the materials. Both the microcomposite and the untreated nanocomposite show a peak at ~54 °C. For the base polymer, a peak appears in a similar temperature region and is referred to as the C_4 peak [19], which originates from the amorphous–crystalline interface of the polymer. However, at higher temperatures, the TSC spectra for the microcomposite and untreated nanocomposite are different. The smaller peak at 78 °C for the untreated nanocomposite is overshadowed by a rapid increase in current in the microcomposite. This increase in current is attributed to Maxwell–Wagner interfacial polarization and this peak is identified as the ρ-peak. Charges trapped at the interface of microparticles are responsible for such peaks [1]. Figure 6 also depicts the TSC spectra for the surface treated nanocomposites. The TES nanocomposite which shows a peak at similar temperature to the C_4-peak shown by the untreated nanocomposites, but shifted upward ~5 °C. The shift in the peak is attributed to the higher viscosity of TES nanocomposites compared to the base polymer and the untreated nanocomposites (not shown here). The height of the peak for the TES nanocomposites is roughly similar to that of the untreated nanocomposite. The AEAPS and HMDS treated composites show similar behavior to the untreated nanocomposite at low temperatures, but the C_4 peak is shifted slightly to lower temperatures (51 °C for the AEAPS nanocomposites and 47 °C for the HMDS nanocomposite). At higher temperatures, however, they both show a clear

Table 5 Trap depths in all composites calculated using initial rise method from the TSC spectra

Samples	Trap depth (eV)	
	C5 peak	C4 peak
Untreated nanocomposite	0.37 ± 0.1	1.1 ± 0.1
Microcomposite	0.35 ± 0.1	1.1 ± 0.1
Vinylsilane-treated nanocomposite	0.41 ± 0.1	1.12 ± 0.1
Aminosilane-treated nanocomposite	2.4 ± 0.1	1.12 ± 0.1
HMDS-treated nanocomposite	2.0 ± 0.1	1.14 ± 0.1

peak at 91 °C, much different from the microcomposite peak and the other nanocomposites. These may originate from the charge carriers trapped by the polar surface groups. Such groups will create surface states with deep trap sites.

To investigate the nature of the trapping, the depth of the trap sites was evaluated using the 'initial rise method' [26]. A temperature range of 0.95–0.98 T_m (where T_m represents the temperature where a TSC peak is observed for a particular sample) was selected for evaluation of trap depth, as this range is likely to give the best accuracy of the results [26]. The trap depth was determined from the slope of an Arrhenius plot. Trap depths evaluated using the above method for both the TSC peaks for all the composites are shown in Table 5. The trap depth for all the C_4 peaks for all samples is roughly similar. However, the trap depth for the second peak of the AEAPS and HMDS nanocomposites is significantly higher than for the other composites for which the feature is only just discernible. These two surface-treated nanocomposites showed a large peak that dwarfs the structure seen in this region for all other composites, which was ascribed to the formation of novel trap sites due to the polar nature of the surface modifier groups. The depth of these traps is also similar to the trap-depth introduced by amine molecules in polyethylene [27], indicating that the silane coupling agents introduce new trap sites.

Figure 7 shows the absorption current derived for a 2 kV/mm step change in electric field for all the composites at room temperature over a period of 10^4 s. The absorption current is seen to conform to the following empirical rule

$$I(t) = A(t)t^{-n}, \tag{5}$$

where I is the current, t is the time after application of the voltage, $A(t)$ is a temperature dependent factor and n is the slope of the bi-log plot. The most significant feature of Fig. 7 is the behavior of the unfilled XLPE and the microcomposite between 200 s and 300 s. They both exhibit a characteristic reduction in slope, which

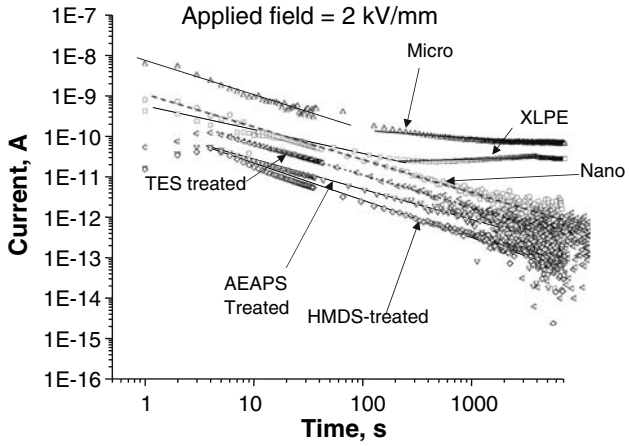

Fig. 7 Absorption current for XLPE and all its composites at an applied field of 2 kV mm^{-1}

is attributed to interfacial polarization [28]. This behavior is observed only in the base polymer and the microcomposite up to an applied field of 10 kV/mm.

The mobility of the charge carriers may be estimated using the method documented by Malec et al. [14].

$$\mu = \frac{0786d^2}{t_p V}, \tag{6}$$

where μ is the mobility of the charge carriers, d is the sample thickness, t_p is the time at which absorption current is at its maximum (peak), and V is the applied voltage. This method relies on the transient space charge limited current characteristics in polyethylene which generates a peak in the current at a given time, t_p, due to the arrival of a space charge front following transport from the source electrode [29]. Such peaks may be seen in Fig. 7 at 2 kV/mm, but become more pronounced at higher fields. The calculated mobility of the charge carriers within a field range of 0.1–9 kV/mm is shown in Fig. 8. For all the nanocomposites the mobility decreases while for the microcomposite and the base polymer it increases with applied field. The mobility of the charge carriers, also, decreased with particle loading suggesting that nanoparticles scatter the carriers reducing their mobility.

Space charge measurements were also reported earlier for some of these materials [30]. Figure 9 shows the image charge versus applied field for the space charge measurements. The point at which the data begins to deviate from linearity is the point at which charge injection occurs. Table 6 shows the onset field for charge injection for each of the materials tested. It

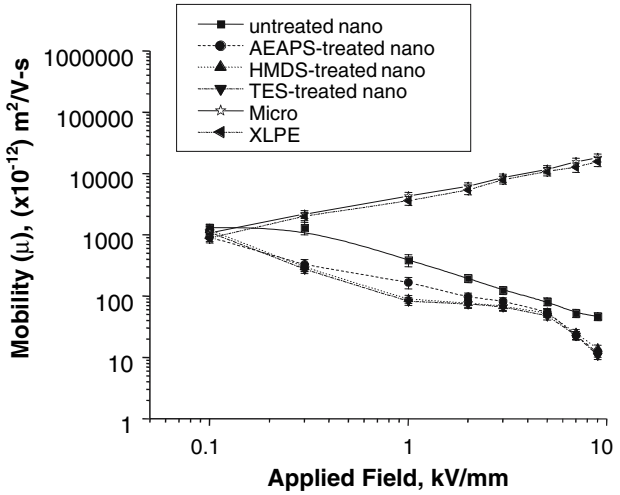

Fig. 8 Carrier mobility as a function of time for XLPE and all its composites

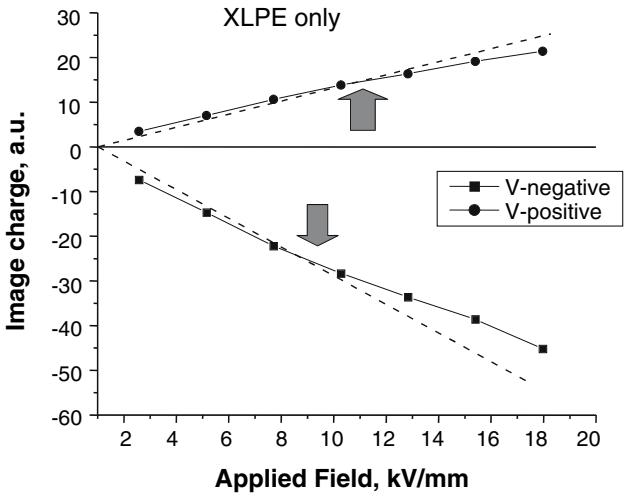

Fig. 9 Image charge accumulation from a PEA experiment on XLPE showing the departure from linearity [28]

Table 6 Threshold field for charge accumulations in front of both the electrodes derived from pulsed electroacoustic analysis [28]

Sample	Threshold field (positive) kV/mm	Threshold field (negative) kV/mm
XLPE	13	–13
XLPE + Micron Scale silica	15	–13
XLPE + untreated nanoscale silica	12	–14
XLPE + AEAPS treated nanoscale silica	–	–
XLPE + HMDS treated nanoscale silica	29	–29
XLPE + TES treated nanoscale silica	25	–26

is clear that surface modification of the nanoparticles resulted in a significant resistance to charge injection, presumably as a result of a change in the work function created by the surface layers.

Discussion

There are three properties that all the nanocomposites have in common. The first is that they all increase the DC dielectric breakdown strength and voltage endurance compared to the unfilled and micron filled composite. The second is that they all have reduced electrical mobility compared to the unfilled and micron filled composite. This could have two origins:

(a) the large number of small particles and thus the large interfacial area may act as scattering centers.
(b) the nanoparticles may alter the crystalline morphology providing another mechanism for scattering (This is particularly so for the TES modified material for which some nucleation is likely).

While, it is established that the degree of crystallinity is not, in itself, significant in controlling the behavior in these systems, charge carriers in the base polymer can move more easily through the crystalline phase than the amorphous phase owing to the ordered structure of the crystalline regions [13]. One may speculate that the particles within the crystalline phase tend to disrupt the continuity of the path provided to the charge carriers, thereby increasing the breakdown strength. A reduction in mobility in the microcomposite was not observed probably because the micron scale fillers are too large to be incorporated within the spherulitic structure and there are far fewer of them to cause scattering.

A third commonality is the presence of larger defects in the micron scale composites compared to the nanocomposites. To understand the effect of defects in determining the breakdown strength of the composites, when a chain scission mechanism is operational as proposed by Artbauer [31], an analysis of breakdown strength dependent on size of the defect can be conducted. Such defects might originate either in the bulk of the polymer or in the interface regions of the particles and the polymer. These defects tend to have a size distribution, and the maximum size of the defect present (rather than the average size of the defects) is critical in determining the breakdown strength. If the distribution is assumed to be exponential in nature, representing the reality that there will be

a few very large size defects, the probability of finding a defect of size l would be given by:

$$g(l) = l_{av} \exp\left(-\frac{l}{l_{av}}\right), \quad (7)$$

where l_{av} is the average size of the defects. According to a chain scission mechanism, failure of the composite will happen when the size of the defect is larger than a critical value (l_c), i.e., $l > l_c$. Also, the size of the defect is inversely proportional to the breakdown strength of the composite (i.e., $l \propto 1/E$). From Eq. (7) the probability of survival ($P_S = 1 - P_F$) can be demonstrated as [15]:

$$P_S = 1 - P_F = \exp\left[-N_c \exp\left(-\frac{l}{l_{av}}\right)\right], \quad (8)$$

where N_c is the total number of defects and l needs to be at least equal to l_c. Following the inverse relation between l and E, that is $El \propto 1$ (a constant); Equation (8) can be re-written as:

$$1 - P_F = \exp\left[-N_c \exp\left(-\frac{El}{E_c l_{av}}\right)\right]. \quad (9)$$

Equation 9 suggests that by replotting the breakdown data (that has reached its E_c) in the form of ln(–ln[1 – P_F]) versus $1/E$ should give the information about the size of the defects. Such a plot is shown in Fig. 10, where the data points originating from the set of breakdown measurements of one type of sample fall onto a line. However, the slope of the fitted line for the microcomposite is significantly lower than both the nanocomposites and the base resin. Since the slope represents the size of the defects, this suggests that the microcomposite must have a much larger defect size distribution than the nanocomposites and the base polymer.

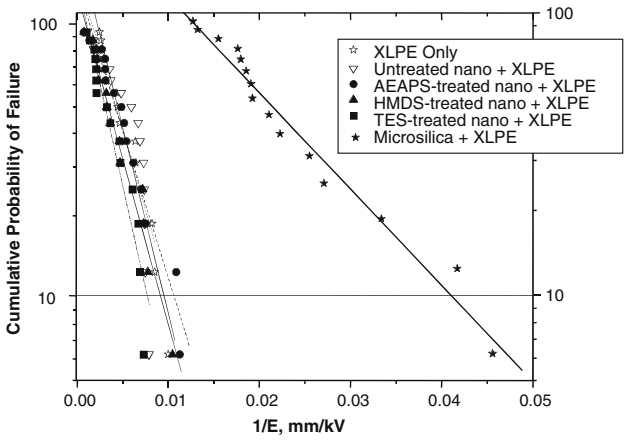

Fig. 10 Failure probability as a function of reciprocal field for all materials

It now remains to discuss the differences between the nanocomposites due to functionalization. These differences, however, must be a minority effect as they do not lead to the order of magnitude effects seen due to the incorporation of nanofillers. Consider first the untreated nanocomposite. In this case, the dielectric spectroscopy results hint at a ''quasi-conductive'' layer [9]. This is supported by the very high oxygen defect concentration (Table 1) and the higher absorption current compared to the other nanocomposites. In this case, the quasi-conductive layer probably modifies the breakdown strength by creating local conductivity that might be expected to reduce the internal space charge. Because of the low concentration of filler, these locally conductive regions do not overlap and thus do not cause early global breakdown, but provide a mechanism for reducing the local field.

The surface treated nanocomposites do not exhibit this ''quasi-conductive'' layer, but they do exhibit two significant differences compared to the untreated nanofiller. First, the polar surface treatments (AEAPS and HMDS) have shown through TSC to have very deep trap sites. Ieda et al. [14] measured similar trap depths in polyethylene through the introduction of amine groups and so it is likely that this phenomenon is the result of the polar surface modifier groups. In turn, this would suggest that the mobilities shown in Fig. 8 are trap dominated, and it is no coincidence that the lowest mobilities are exhibited by the functionalized materials that provide deep trap sites. The reduced mobility could contribute to increased breakdown strength. Finally, all the surface treated nanofillers exhibit a higher onset field for charge injection. While this data is significant, at this point, the reasons for this behavior are not clear and are currently under investigation.

Conclusions

1. The addition of nanoscale silica to XLPE leads to an order of magnitude increase in breakdown strength compared to micron scale filler, and at least a 20% increase compared to unfilled XLPE. However, at elevated temperature, appropriate functionalization can lead to enhancements in breakdown strength in excess of 175% with this technology.
2. The addition of nanoscale silica to XLPE leads to two orders of magnitude improvement in the voltage endurance compared to unfilled XLPE.

3. The most likely mechanism that could be used to explain the increase in breakdown strength in the nanocomposites is the scattering created by both particle/polymer interfaces and possibly disrupted crystalline structure.
4. The data suggest that the mechanism leading to the decrease in breakdown strength for the micron scale filler is because of the introduction of defects created by the micron scale fillers.
5. The mechanism leading to the subtle differences in breakdown strength due to surface treatment of the nanofillers is either due to the defect reduction via chemical linkage between particle and polymer or, due to the introduction of deep trap sites in the polymer due to the surface modifier groups.

Acknowledgements The authors are grateful to the Electric Power Research Institute for the support of this activity and to Professor Fothergill's research group at the University of Leicester, UK for the contribution of pulsed electroacoustic measurements. Discussions with Dr. Clive Reed on the chemical aspects of this work are also gratefully acknowledged.

References

1. Nelson J, Fothergill JC (2004) Nanotechnology 15:586
2. Ma D, Siegel RW, Hong JI, Schadler LS, Mårtensson E, Önneby C (2004) J Mater Res 19(3):857
3. Nelson JK, Hu Y (2005) J Phys D (Appl Phys) 38:213
4. Nelson JK, Fothergill JC, Dissado LA, Peasgood W (2002) In: Proceedings of the conference on Elec Insul & Dielec Phenom, IEEE, Mexico, pp 295–298
5. Montanari GC, Fabiani D, Palmieri F, Kaempfer D, Thomann R, Mulhaupt R (2004) IEEE Trans Diel Elect Insul 11(5):754
6. Ajayan PM, Braun PV, Schadler LS (2003) In: Nanocomposite Science and Technology, Wiley-VCH Verlag, GmbH&Co. KgaA, Weinham
7. Tanaka T, Montanari GC, Mülhaupt R (2004) IEEE Trans Diel Elect Insul 11/5:763
8. Lewis TJ (1994) IEEE Trans Diel Elect Insul 1:812
9. Lewis TJ (2004) IEEE Trans Diel Elect Insul 11:739
10. Fujita F, Ruike M, Baba M (1996) Conference record of the 1996. IEEE Intl Symp Elec Ins, IEEE, San Francisco 2:738
11. Khalil MS, Henk PO, Henriksen M (1990) Conference record of the 1990 IEEE International Symp on Elec. Insul; IEEE, Montreal, Canada, p 268
12. Fothergill JC, Nelson JK, Fu M (2004) Proceedings of the IEEE Conf on Elect Insul & Diel Phenom, CEIDP, Oct. 17–20. pp 406–409
13. Ma D, Akpalu YA, Li Y, Siegel RW, Schadler LS (2005) J Polym Sci Part B Polym Phys 43(5):463
14. Malec D, Truong H, Essolbi R, Hoand TG (1998) IEEE Trans Diel Elect Insul 5/2:301
15. Roy M, Nelson JK, MacCrone RK, Schadler LS, Reed CW, Keefe R, Zenger W (2005) IEEE Trans Diel Elect Insul 12:629
16. Lunsford JH (1973) Catal Rev 8(1):135
17. Canet D (1996) Nuclear magnetic resonance: concepts and methods. John Wiley & Sons Inc., Chichester, New York
18. Dissado LA, Fothergill JC (1992) Electrical degradation and breakdown in polymers. Peter Peregrinus Ltd
19. Ieda M, Mizutani T, Suzuoki Y (1980) Polymers, Memoirs of the Faculty of Engineering, Nagoya University, 32/2
20. Peacock JA (2000) Handbook of polyethylene: structures, properties and applications. Marcel Dekker, New York
21. Lichtenecker K, Rother K (1931) Phys Zeit 32:255
22. Maxwell-Ganet JC (1904) Philos Trans Roy Soc Lond Ser A 203:385
23. Landau LD, Lifshitz EM (1984) Electrodynamics of continuous media, 2nd edn. Pergamon Press, Oxford
24. Jonscher AK (1983) Dielectric relaxation of solids. Chelsea Dielectric Press
25. O'Konski J (1960) J Phys Chem 64:605
26. Maeta S, Sakaguchi K (1980) Jpn J Appl Phys 19/3:519
27. Van Turnhout J (1975) Thermally stimulated discharge for polymer electrets. Elsevier, Amsterdam
28. Raju GG (2003) Dielectrics in electric fields. Marcel Dekker, New York
29. Many A, Rakavy G (1962) Theory of transient-space-charge-limited currents in solids in the presence of trapping. Phys Rev 126/6:1980
30. Roy M, Nelson JK, Schadler LS, Zou C, Fothergill JC (2005) Ann Rep conf on Electrical Insulation and Dielectric Phenomenon, IEEE, pp 183–186
31. Artbauer J (1996) J Phys D Appl Phys 29:446